Accepted (peer-reviewed) version

Vacuum deposited triple-cation mixed-halide perovskite solar cells

*Lidón Gil-Escrig,‡ Cristina Momblona,‡ Maria-Grazia La-Placa, Pablo P. Boix, Michele Sessolo and Henk J. Bolink**

‡These authors contributed equally to this work.

Instituto de Ciencia Molecular
Universidad de Valencia
C/ J. Beltrán 2, 46980, Paterna, Spain
E-mail: henk.bolink@uv.es

Keywords: perovskite, wide bandgap, vacuum deposition, doping, mixed cation

Abstract

Hybrid lead halide perovskites are promising materials for future photovoltaics applications. Their spectral response can be readily tuned by controlling the halide composition, while their stability is strongly dependent on the film morphology and on the type of organic cation used. Mixed cation and mixed halide systems have led to the most efficient and stable perovskite solar cells reported, so far prepared exclusively by solution-processing. This might be due to the technical difficulties associated with the vacuum deposition from multiple thermal sources, requiring a high level of control over the deposition rate of each precursor during the film formation. In this report, we use multiple sources (3 and 4) thermal vacuum deposition to prepare for the first time multi-cations/anions perovskite compounds. These thin-film absorbers were implemented into fully vacuum deposited solar cells using doped organic semiconductors. A maximum power conversion efficiency (PCE) of 16 % was obtained, with promising device stability. We highlight the importance of the control over the film morphology, which differs substantially when these compounds are vacuum processed. Avenues to improve the

morphology and hence the performance of fully vacuum processed multi-cations/anions perovskite solar cells are proposed.

Lead halide perovskite compounds represents a major breakthrough in modern photovoltaics (PV). The archetypical organic-inorganic (hybrid) perovskite can be described with the ABX_3 structure, where A is a monovalent organic or inorganic cation e.g. methylammonium (MA^+ or $CH_3NH_3^+$), formamidinium (FA^+ or $NH_2CH{=}NH_2^+$) or cesium (Cs^+), B is a divalent metal cation (Pb^{2+} or Sn^{2+}) and X is a halide (Cl^-, Br^-, I^-).[1-3] The most widely studied perovskite solar cells, based on $MAPbI_3$, have achieved power conversion efficiency (PCE) exceeding 20%.[4, 5] Besides efficiency, long-term stability is a basic requirement in view of a potential commercialization of these devices. Many studies have highlighted the possible degradation sources reported for $MAPbI_3$-based solar cells, such as moisture, light soaking and thermal degradation.[6-8] The device stability can be enhanced by using more stable electron and hole transporting layers, chemical inhibition or passivation layers.[9-12] In parallel, the use of additives and compositional engineering (or alloying) using mixtures of different cations and/or halides have proved to be a successful route to mitigate the material instability.[13-16]Although the substitution of MA^+ with FA^+ or Cs^+ in $MAPbI_3$ leads to compounds with band gaps interesting for photovoltaics, ~1.45 and ~1.75 eV, respectively, both materials present polymorphism.[17-20] $FAPbI_3$ and $CsPbI_3$ have a wide band gap non-perovskite δ- or "yellow" phase and a photoactive perovskite α- or "black" phase. The δ → α transition is reported to take place at temperatures roughly above 160 ºC for $FAPbI_3$ and at 300 ºC for $CsPbI_3$.[21] Unfortunately, the reversible slow phase transition at room temperature of the α-$FAPbI_3$ leads to unstable device operation. In order to stabilize the α-phase, solid-state alloys composed of a mixture of different A cations (Rb/Cs/MA/FA) and/or X anions (Br/I) have been reported.[15, 16, 22, 23] In general for lead iodide-based perovskites, binary A cation mixtures such as (FA/MA), (MA/Cs), (FA/Cs) and (FA/Rb) lead to enhanced stability compared to the single cation MA^+ or FA^+ perovskites. On the other hand, binary X anion mixtures such as MAPb(I/Br) and FAPb(I/Br) suffer from phase-segregation into I- and Br-rich domains under light exposure.[24],[25] The addition of Cs^+ in the FAPb(I/Br) system has been reported to suppress this halide segregation.[16] The coordinated use of these strategies (mixed cation and mixed halide systems) has led to the most efficient and stable perovskite solar cells reported so far, with champion devices exhibiting efficiency exceeding 22.1%.[14, 15, 26]

Up to now the compositional engineering of perovskite absorbers has relied solely on solution-process methods. On the other hand, vacuum deposited perovskite solar cells have also been reported, obtaining efficiencies that compete with their solution-processed counterparts.[4, 27, 28] Vacuum deposition methods are widely implemented into the semiconductor industry and present important advantages over solution-based techniques, such as fabrication of high purity films, compatibility with large areas and fine control over film thickness. These techniques eliminates issues related to the use of solvents, such as toxicity, solubility limitation of precursors or the need of orthogonal solvents in order to process multilayer devices. Moreover, the low fabrication temperature makes vacuum deposition compatible with a wide range of substrates, including textiles, textured or flexible substrates. In addition to $MAPbI_3$ films, also mixed halide inorganic perovskites such as $CsPbIBr_2$ and the narrow bandgap $FAPbI_3$ compound have been reported.[29, 30] To date, however, there are still no reports on vacuum deposited multi-cation and multi-halide perovskites. This might be due to the technical difficulties associated with the vacuum deposition from multiple thermal sources, requiring a high level of control over the deposition rate of each precursor during the film formation. In this report, we use multiple sources (3 and 4) thermal vacuum deposition to prepare for the first time multi-cations/anions perovskite compounds of the type $APb(Br_xI_{1-x})_3$, with A being Cs, MA and FA. These thin-film absorbers were implemented into fully vacuum deposited solar cells using doped organic semiconductors. A maximum power conversion efficiency (PCE) of 16 % was obtained, with promising device stability. We highlight the importance of the control over the film morphology, which differs substantially when these compounds are vacuum processed. Avenues to improve the morphology and hence the performance of fully vacuum processed multi-cations/anions perovskite solar cells are also discussed.

The mixed-cation lead mixed-halide perovskite thin films were prepared by simultaneous thermal vacuum deposition of the precursor compounds, MAI, CsBr, FAI and PbI_2. Prior to perovskite deposition, the starting materials were individually sublimed and a calibration factor was obtained by comparing the thickness detected from the quartz crystal microbalance (QCM) sensors with that measured with a mechanical profilometer. The details of the experimental conditions are provided in the Supporting Information. Energy dispersive X-ray analysis (EDX) was used to estimate the stoichiometry of the resulting perovskite films, indicating a I/Br ratio of about 5. This ratio has been chosen following previous reports on similar systems.[15] Hence, double-cation mixed halide perovskite films with composition $Cs_{0.5}FA_{0.5}Pb(I_{0.83}Br_{0.17})_3$ were initially deposited and characterized. The UV-Vis absorption spectrum of this compound (**Figure 1**a) shows an absorption onset corresponding to an optical bandgap of 1.62 eV,

estimated from the Tauc plot (Figure S1). The X-ray (XRD) diffraction of the double-cation perovskite (Figure 1b) present the expected perovskite pattern, with intense signals at 14.1º and 28.3º corresponding to the (100) and (200) directions. On the other hand, the small component at 11.5º might be due to a residual δ-phase in the $Cs_{0.5}FA_{0.5}Pb(I_{0.83}Br_{0.17})_3$ film.[14, 31]As previously reported, the incorporation of MA cation in mixed compounds can help the formation and stabilization of the α-phase.[31] This effect has been attributed to the larger dipole of the MA cation leading to a stronger interaction with the lead halide octahedral cage.[31, 32] For this reason, we prepared triple-cation mixed halide perovskite films by simultaneous vacuum deposition of MAI, CsBr, FAI and PbI_2. As expected, after MA^+ addition the δ-phase seems to be suppressed, as no apparent signal at low angle is displayed in the XRD (Figure 1b). As compared to the double-cation perovskite, the optical bandgap of the triple-cation compound was estimated to be about 1.70 eV (Figure S1), the blue-shift resulting from partial substitution of FA with MA.[33] The optical absorption of the triple-cation $Cs_{0.5}FA_{0.4}MA_{0.1}Pb(I_{0.83}Br_{0.17})_3$ perovskite layer was monitored during continuous exposure to air at 25 ºC and 40% relative humidity, and was found to be unaltered for days (Figure S2). This indicates an enhanced stability towards the environmental agents of this vacuum deposited perovskite formulation.

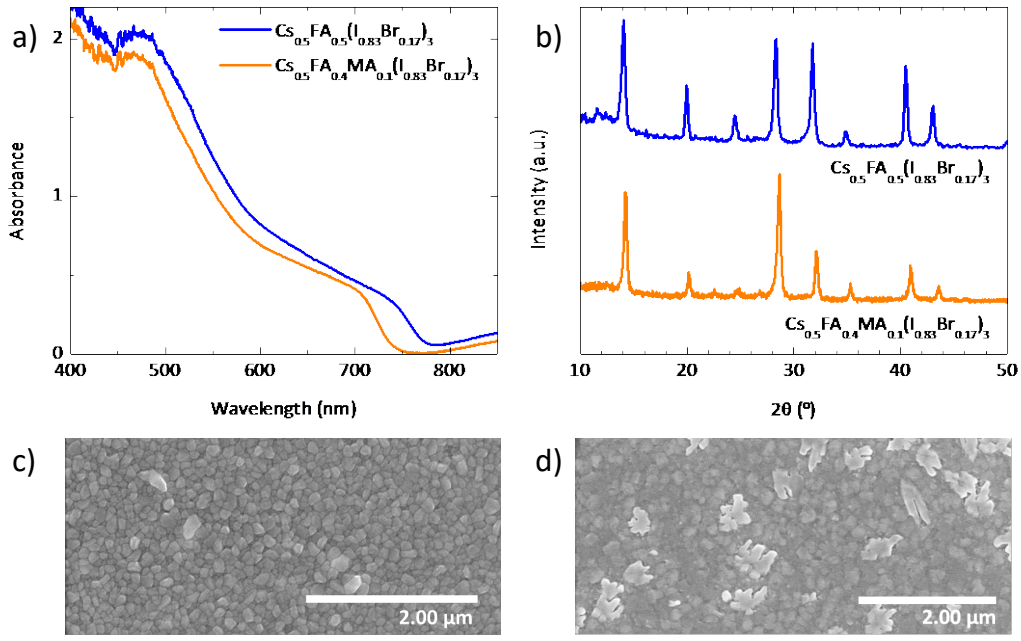

Figure 1.a) UV-Vis absorption spectra and b) GIXRD patterns of vacuum deposited multi-cations mixed halide perovskite thin films. SEM images of the c) double- and d) triple-cation perovskite layers.

The top-view scanning electron microscopy (SEM) images of the double- and triple-cation perovskites (Figure 1c and 1d) show complete surface coverage, with compact and uniform morphology and grain size ranging from 100 to 200 nm. Some larger irregular crystals are present on the top of the triple-cation $Cs_{0.5}FA_{0.4}MA_{0.1}Pb(I_{0.83}Br_{0.17})_3$ perovskite, which are most likely related to the presence of MA. Their appearance might indicate a partial segregation of this compound or of perovskite crystals with higher MA content.

The double- and triple-cation perovskite films were used as absorbers in planar n-i-p solar cell, using organic semiconductors as charge transport materials (**Figure 2**a).The n- and p-type contact semiconductors consist of double-layers, formed by a thick doped layer (40 nm) (n-ETL, p-ETL) and a thinner intrinsic film in contact with the perovskite (10 nm). The electron and hole transporter material (ETL, HTL) were fullerene (C_{60}) and N4,N4,N4",N4"-tetra([1,1'-biphenyl]-4-yl)-[1,1':4',1"-terphenyl]-4,4"-diamine (TaTm), while the dopants employed were N1,N4-bis(tri-p-tolylphosphoranylidene) benzene-1,4-diamine (PhIm) and 2,2′-(perfluoronaphthalene-2,6-diylidene) dimalononitrile (F_6-TCNNQ), respectively. The dopant concentration was 60 wt% for PhIm and 11 wt% for F_6-TCNNQ,[4] which is adequate to ensure sufficient conductivity in the n-ETL and p-HTL, respectively. The n-i-p configuration was selected due to its superior PV performance compared to their p-i-n counterpart, which is related to the higher conductivity of the n-ETL at the front contact.[4] For each perovskite composition and thickness, at least two solar cells each containing four pixels were evaluated.

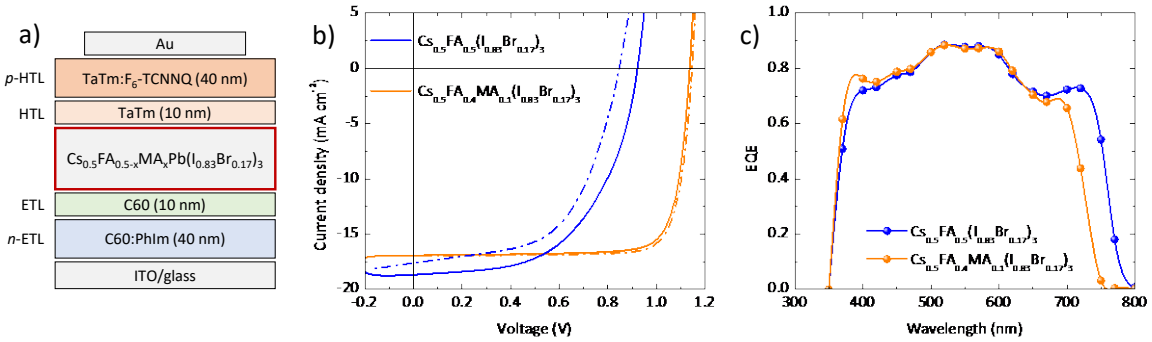

Figure 2. a) n-i-p device structure. b) J-V curve under 100 mW cm^{-2} illumination (forward scan: solid line; reverse scan: dashed line) and c) spectral response for the best solar cells obtained using double- and triple-cation perovskite absorbers (thickness of 310 nm and 340 nm, respectively).

The current-voltage (J-V) characteristics and the corresponding external quantum efficiency (EQE) of the champion solar cells employing $Cs_{0.5}FA_{0.5}Pb(I_{0.83}Br_{0.17})_3$ and

$Cs_{0.5}FA_{0.4}MA_{0.1}Pb(I_{0.83}Br_{0.17})_3$ absorbers are reported in Figure 2b-c. The device performance parameters extracted from the characterization are summarized in **Table 1**. The double-cation perovskite based solar cell exhibited a large short-circuit current density (J_{SC}) of 18.7 mA cm^{-2}, which is remarkable considering the thickness of the absorber (310 nm).This is in accordance with the high spectral response of the cell, ranging between 0.7 and 0.85 over the whole visible spectrum (Figure 2c). The fill factor (FF) extracted from the J-V curves recorded in forward and reverse bias (fwd and rev; from short circuit to open circuit and vice versa) is, however, very low (56-57%). This indicates a hindered charge collection and/or a substantial charge recombination within the device. The latter hypothesis is also supported by the low open circuit voltage (V_{oc}), 922 mV and 846 mV in forward and reverse bias, respectively. The power efficiency is overall rather limited, ranging from 8.5% to 9.7% when the cell is measured in forward and reverse bias, respectively. Moreover, in contrast with vacuum deposited $MAPbI_3$ solar cells with analogous configuration,[4] the device based on this double-cation perovskite shows also large hysteresis among the forward and reverse scan. These observations might arise from the persistence of a residual δ-phase, as discussed above. Upon substitution of FA with MA in the triple-cation perovskite, only negligible hysteresis between forward and reverse scans was observed, and the J-V characteristics is substantially recovered. The V_{oc} increases up to 1140 mV and the FF is enhanced from 56 to 81%, indicating an efficient rectification of the perovskite diode. The record PCE for the vacuum deposited triple-cation mixed halide perovskite solar cells is 16.0%, with the limiting factor being the J_{SC} (16.9 mA cm^{-2}).The photocurrent reduction is expected as the reduced FA content results in an enlarged bandgap. In order to improve the J_{SC}, a series of solar cells based on the triple-cation perovskite $Cs_{0.5}FA_{0.4}MA_{0.1}Pb(I_{0.83}Br_{0.17})_3$ with increasing absorber thickness was fabricated. The optical absorption, XRD patterns and top-view SEM images of the resulting perovskite films are shown in Figure S3. It is worth to note how the optical bandgap is essentially unvaried (1.70 eV) with increasing layer thickness (Figure S1). This indicates that the absolute and relative deposition rates of the four precursors are extremely stable during the deposition of the mixed cation/anion perovskite. The main difference among films with different thickness was found in their morphology. From the SEM images (Figure S3c-e), large crystals with different sizes appears on the film surface, without an evident correlation with the thickness nor with the corresponding XRD patterns. The J-V characteristics and EQE spectra for n-i-p solar cells based on the triple-cation perovskite films with increasing thickness are reported in **Figure 3** and the PV parameters are summarized in Table 1. The corresponding statistical analysis is reported in Figure S4.

Table 1. PV performance parameters extracted from the J-V characteristics of n-i-p solar cells employing vacuum deposited double- and triple-cation perovskites.

Perovskite	thickness [nm]		V_{OC} [mV]	J_{SC} [mAcm^{-2}]	*FF* [%]	*PCE* [%]
$Cs_{0.5}FA_{0.5}Pb(I_{0.83}Br_{0.17})_3$	310	*fwd*	922	18.7	56	9.7
		rev	846	17.6	57	8.5
$Cs_{0.5}FA_{0.4}MA_{0.1}Pb(I_{0.83}Br_{0.17})_3$	340	*fwd*	1137	16.9	81	15.6
		rev	1146	17.0	82	16.0
	430	*fwd*	1089	15.8	76	13.1
		rev	1089	15.7	78	13.3
	600	*fwd*	1022	15.5	51	8.1
		rev	1022	15.8	58	9.4

Despite the obvious increase in light absorption observed in the UV-Vis spectra (Figure S3), the corresponding photocurrent does not increase, in contrast it was found to diminish with increasing absorber thickness. Interestingly, with thicker perovskite absorbers the spectral response was found to be lower in the high energy region (400 - 550 nm), but enhanced in the red part of the visible spectrum. This phenomenon might be due to an unbalanced hole and electron mobility of the vacuum deposited triple-cation absorber. Blue photons are absorbed close to the front contact, and the photogenerated positive carriers have to travel through the whole absorber to be collected at the back HTL. On the contrary, red photons will penetrate deeper in the film, hence the electrons should be transported all the way to the front n-type contact. Therefore, the EQE trend suggests slightly unbalanced diffusion lengths for both carriers in our perovskite films, as previously discussed upon cation variation by other methods.[19] This can also partially explain the reduction in V_{oc} and FF observed with thicker absorbers, where recombination would be enhanced.

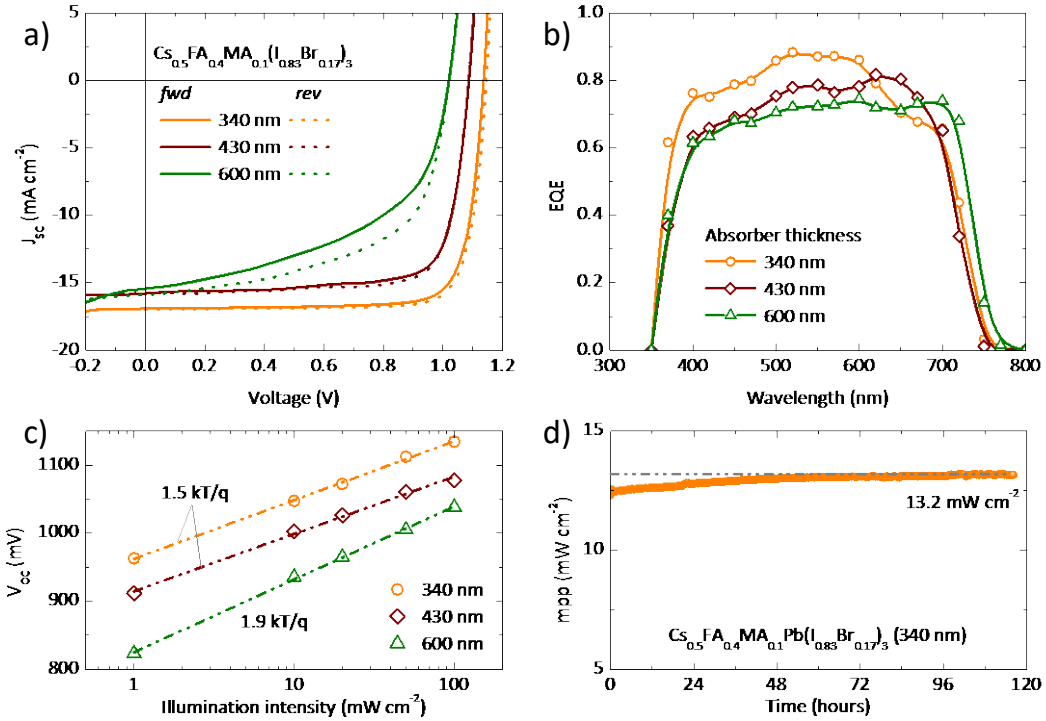

Figure 3.a) J-V characteristics under 100 mW cm^{-2} illumination, b) EQE spectra and c) light intensity dependence of the photovoltage for the triple-cation perovskite solar cells series. d) Maximum power point tracking over 5 days for an unencapsulated device with perovskite thickness of 430 nm, measured in inert atmosphere.

In order to further understand the losses associated with thicker perovskite absorbers, the light intensity (I) dependence of the J-V curves was measured. The linear dependence of J_{SC} with I (Figure S5) denotes that there are no significant energy barriers in the device, and minimal space-charge limited effects.[34] The light intensity dependence of V_{oc} is reported in a semilogaritmic scale in Figure 3c. From the slope of the linear fitting of V_{OC} vs ln(I) graph, we extracted ideality factors of 1.5, 1.5 and 1.9k_BT/q for the solar cells with 340, 450 and 600 nm thick perovskite layers, respectively. Hence in thicker films, the ideality factors closer to 2 together with the lower photovoltage suggest a predominant trap-assisted recombination in the bulk of the absorber.[35, 36] The presence of traps can also be deduced from the trend of the FF vs. I (Figure S5), as it diminishes at lower photocarrier generation. Apart from these consideration, one should also take into account the morphology of the triple-cation perovskite films, which shows the uneven growth of irregular and large structures superimposed on the fine polycrystalline perovskite surface. Finally, the solar cells with thinner absorber were tested under continuous 1 sun illumination inside a nitrogen-filled glovebox. The maximum power

point (mpp) tracking of a representative cell with triple-cation perovskite absorber at 430 nm thickness at 25 ºC and without UV filter is reported in Figure 3d, showing no signs of degradation up to 5 days of continuous illumination.

In summary, we prepared double- and triple-cation, mixed halide perovskites by simultaneous thermal vacuum deposition of up to four precursors. The composition and bandgap can be finely tuned and can be chosen in view of specific applications (i.e. single junction or tandem solar cells). n-i-p planar solar cells based on these materials show promising efficiencies, up to 16% in the case of the triple cation $Cs_{0.5}FA_{0.4}MA_{0.1}Pb(I_{0.83}Br_{0.17})_3$ absorber. We observed an uneven morphology which is in contrast with previous reports on vacuum deposited simpler perovskite stoichiometry. Considering the importance of the homogeneity, grain size and crystallinity, on the optoelectronic properties of hybrid perovskites, much improved PV performances are expected by further controlling their morphology. This can be achieved by i) modification of the perovskite composition, ii) favoring crystallization through the control of the substrate temperature, or iii) by post-treatment (thermal or chemical) of the as-deposited compounds. The results presented here are very promising and validate vacuum deposition as a powerful technique to fabricate efficient and stable mixed-cation mixed-halide perovskite solar cells.

Acknowledgment

We are grateful to Jorge Ferrando for his assistance with the sample characterization. Financial support is acknowledged from the European Union H2020 project INFORM (grant 675867), the Spanish Ministry of Economy and Competitiveness (MINECO) via the Unidad de Excelencia María de Maeztu MDM-2015-0538 and MAT2014-55200, PCIN-2015-255 and the Generalitat Valenciana (Prometeo/2012/053). M.G.L.P. acknowledges support from a Grisolia grant (GRISOLIA/2015/A/146). C.M., M.S. and P.P.B. thank the MINECO for their pre- and post-doctoral (JdC and RyC) contracts.

References

[1] C. C. Stoumpos, M. G. Kanatzidis, *Adv. Mater.* **2016**, *28*, 5778.
[2] Y. Zhao, K. Zhu, *Chem. Soc. Rev.* **2016**, *45*, 655.
[3] D. Zhao, Y. Yu, C. Wang, W. Liao, N. Shrestha, C. R. Grice, A. J. Cimaroli, L. Guan, R. J. Ellingson, K. Zhu, X. Zhao, R.-G. Xiong, Y. Yan, *Nat. Energy* **2017**, *2*, 17018.
[4] C. Momblona, L. Gil-Escrig, E. Bandiello, E. M. Hutter, M. Sessolo, K. Lederer, J. Blochwitz-Nimoth, H. J. Bolink, *Energy Environ. Sci.* **2016**, *9*, 3456.
[5] D.-Y. Son, J.-W. Lee, Y. J. Choi, I.-H. Jang, S. Lee, P. J. Yoo, H. Shin, N. Ahn, M. Choi, D. Kim, N.-G. Park, *Nat. Energy* **2016**, *1*, 16081.

[6] A. M. A. Leguy, Y. Hu, M. Campoy-Quiles, M. I. Alonso, O. J. Weber, P. Azarhoosh, M. van Schilfgaarde, M. T. Weller, T. Bein, J. Nelson, P. Docampo, P. R. F. Barnes, *Chem. Mater.* **2015**, *27*, 3397.
[7] B. Conings, J. Drijkoningen, N. Gauquelin, A. Babayigit, J. D'Haen, L. D'Olieslaeger, A. Ethirajan, J. Verbeeck, J. Manca, E. Mosconi, F. D. Angelis, H.-G. Boyen, *Adv. Energy Mater.* **2015**, *5*, 1500477.
[8] H. Yuan, E. Debroye, K. Janssen, H. Naiki, C. Steuwe, G. Lu, M. Moris, E. Orgiu, H. Uji-i, F. De Schryver, P. Samorì, J. Hofkens, M. Roeffaers, *J. Phys. Chem. Lett.* **2016**, *7*, 561.
[9] H. Back, G. Kim, J. Kim, J. Kong, T. K. Kim, H. Kang, H. Kim, J. Lee, S. Lee, K. Lee, *Energy Environ. Sci.* **2016**, *9*, 1258.
[10] X. Jin, X. Lei, C. Wu, G. Jiang, W. Liu, H. Zeng, T. Chen, C. Zhu, *J. Mater. Chem. A* **2017**, *5*, 19884.
[11] H. Tan, A. Jain, O. Voznyy, X. Lan, F. P. García de Arquer, J. Z. Fan, R. Quintero-Bermudez, M. Yuan, B. Zhang, Y. Zhao, F. Fan, P. Li, L. N. Quan, Y. Zhao, Z.-H. Lu, Z. Yang, S. Hoogland, E. H. Sargent, *Science* **2017**, *355*, 722.
[12] G. S. Han, J. S. Yoo, F. Yu, M. L. Duff, B. K. Kang, J.-K. Lee, *J. Mater. Chem. A* **2017**, *5*, 14733.
[13] X. Li, M. Ibrahim Dar, C. Yi, J. Luo, M. Tschumi, S. M. Zakeeruddin, M. K. Nazeeruddin, H. Han, M. Grätzel, *Nat. Chem.* **2015**, *7*, 703.
[14] N. J. Jeon, J. H. Noh, W. S. Yang, Y. C. Kim, S. Ryu, J. Seo, S. I. Seok, *Nature* **2015**, *517*, 476.
[15] M. Saliba, T. Matsui, J.-Y. Seo, K. Domanski, J.-P. Correa-Baena, M. K. Nazeeruddin, S. M. Zakeeruddin, W. Tress, A. Abate, A. Hagfeldt, M. Gratzel, *Energy Environ. Sci.* **2016**, *9*, 1989.
[16] D. P. McMeekin, G. Sadoughi, W. Rehman, G. E. Eperon, M. Saliba, M. T. Hörantner, A. Haghighirad, N. Sakai, L. Korte, B. Rech, M. B. Johnston, L. M. Herz, H. J. Snaith, *Science* **2016**, *351*, 151.
[17] M. R. Filip, G. E. Eperon, H. J. Snaith, F. Giustino, *Nat. Commun.* **2014**, *5*, 5757.
[18] D. B. Mitzi, *J. Mater. Chem.* **2004**, *14*, 2355.
[19] G. E. Eperon, S. D. Stranks, C. Menelaou, M. B. Johnston, L. M. Herz, H. J. Snaith, *Energy Environ. Sci.* **2014**, *7*, 982.
[20] T. M. Koh, K. Fu, Y. Fang, S. Chen, T. C. Sum, N. Mathews, S. G. Mhaisalkar, P. P. Boix, T. Baikie, *J. Phys. Chem. C* **2014**, *118*, 16458.
[21] C. C. Stoumpos, C. D. Malliakas, M. G. Kanatzidis, *Inorg. Chem.* **2013**, *52*, 9019.
[22] M. Saliba, T. Matsui, K. Domanski, J.-Y. Seo, A. Ummadisingu, S. M. Zakeeruddin, J.-P. Correa-Baena, W. R. Tress, A. Abate, A. Hagfeldt, M. Grätzel, *Science* **2016**, *354*, 206.
[23] T. Matsui, J.-Y. Seo, M. Saliba, S. M. Zakeeruddin, M. Grätzel, *Adv. Mater.* **2017**, *29*, 1606258.
[24] D. J. Slotcavage, H. I. Karunadasa, M. D. McGehee, *ACS Energy Lett.* **2016**, *1*, 1199.
[25] E. T. Hoke, D. J. Slotcavage, E. R. Dohner, A. R. Bowring, H. I. Karunadasa, M. D. McGehee, *Chem. Sci.* **2015**, *6*, 613.
[26] W. S. Yang, B.-W. Park, E. H. Jung, N. J. Jeon, Y. C. Kim, D. U. Lee, S. S. Shin, J. Seo, E. K. Kim, J. H. Noh, S. I. Seok, *Science* **2017**, *356*, 1376.
[27] S.-Y. Hsiao, H.-L. Lin, W.-H. Lee, W.-L. Tsai, K.-M. Chiang, W.-Y. Liao, C.-Z. Ren-Wu, C.-Y. Chen, H.-W. Lin, *Adv. Mater.* **2016**, *28*, 7013.
[28] D. Zhao, W. Ke, C. R. Grice, A. J. Cimaroli, X. Tan, M. Yang, R. W. Collins, H. Zhang, K. Zhu, Y. Yan, *Nano Energy* **2016**, *19*, 88.
[29] C.-Y. Chen, H.-Y. Lin, K.-M. Chiang, W.-L. Tsai, Y.-C. Huang, C.-S. Tsao, H.-W. Lin, *Adv. Mater.* **2017**, *29*, 1605290.

[30] J. Borchert, R. L. Milot, J. B. Patel, C. L. Davies, A. D. Wright, L. Martínez Maestro, H. J. Snaith, L. M. Herz, M. B. Johnston, *ACS Energy Lett.* **2017**, *2*, 2799.
[31] A. Binek, F. C. Hanusch, P. Docampo, T. Bein, *J. Phys. Chem. Lett.* **2015**, *6*, 1249.
[32] J. M. Frost, K. T. Butler, F. Brivio, C. H. Hendon, M. van Schilfgaarde, A. Walsh, *Nano Lett.* **2014**, *14*, 2584.
[33] N. Pellet, P. Gao, G. Gregori, T.-Y. Yang, M. K. Nazeeruddin, J. Maier, M. Grätzel, *Angew. Chem. Int. Ed.* **2014**, *53*, 3151.
[34] L. J. A. Koster, V. D. Mihailetchi, H. Xie, P. W. M. Blom, *Appl. Phys. Lett.* **2005**, *87*, 203502.
[35] T. S. Sherkar, C. Momblona, L. Gil-Escrig, J. Ávila, M. Sessolo, H. J. Bolink, L. J. A. Koster, *ACS Energy Lett.* **2017**, *2*, 1214.
[36] W. Tress, M. Yavari, K. Domanski, P. Yadav, B. Niesen, J. P. Correa Baena, A. Hagfeldt, M. Graetzel, *Energy Environ. Sci.* **2017**.

Supporting Information

Vacuum deposited triple-cation mixed-halide perovskite solar cells

*Lidón Gil-Escrig,‡ Cristina Momblona,‡ Maria-Grazia La-Placa, Pablo P. Boix, Michele Sessolo and Henk J. Bolink**

Experimental section

Materials. Photolithographically patterned ITO coated glass substrates were purchased from Naranjo Substrates. Fullerene (C_{60}) was purchased from Sigma Aldrich. N1,N4-bis(tri-p-tolylphosphoranylidene)benzene-1,4-diamine (PhIm), N4,N4,N4",N4"-tetra([1,1'-biphenyl]-4-yl)-[1,1':4',1"-terphenyl]-4,4"-diamine (TaTm) and 2,2'-(Perfluoronaphthalene-2,6-diylidene) dimalononitrile (F_6-TCNNQ) were provided from Novaled GmbH. CH_3NH_3I (MAI) was purchased from Lumtec, $NH_2CH{=}NH_2I$ (FAI) from Dyesol, CsBr and PbI_2 from Tokyo Chemical Industry CO (TCI). All materials were used as received.

Device preparation. ITO-coated glass substrates were subsequently cleaned with soap, water and isopropanol in an ultrasonic bath, followed by UV-ozone treatment. They were transferred to a vacuum chamber integrated into a nitrogen-filled glovebox and evacuated to a pressure of 10^{-6} mbar for the charge extraction front contact layer deposition. The vacuum chamber for organic deposition is equipped with six temperature controlled evaporation sources (Creaphys) fitted with ceramic crucibles. The sources were directed upwards with an angle of approximately 90° with respect to the bottom of the evaporator. The substrate holder to evaporation sources distance is approximately 20 cm. Three quartz crystal microbalance (QCM) sensors are used, two monitoring the deposition rate of each evaporation source and a third one close to the substrate holder monitoring the total deposition rate. For thickness calibration, we first individually sublimed the charge transport materials and their dopants (TaTm and F_6-TCNNQ, C_{60} and PhIm). A calibration factor was obtained by comparing the thickness inferred from the QCM sensors with that measured with a mechanical profilometer (Ambios XP1). Hence these materials were co-sublimed at temperatures ranging from 135-160 ºC for the dopants to 250 ºC for the pure charge transport molecules, and the evaporation rate was controlled by separate QCM sensors and adjusted to obtain the desired doping concentration. In general, the deposition rate for TaTm and C_{60} was kept constant at 0.8 Å s^{-1} while varying

the deposition rate of the dopants during co-deposition. Pure TaTm and C_{60} layers were deposited at a rate of 0.5 Å s^{-1}. 40 nm thick films of the n-doped electron-transport layer (n-ETL, C_{60}:PhIm, 60 wt%) capped with 10 nm of the pure C_{60} were deposited. After completion of the front contact, the chamber was vented with dry N_2 and the samples were transferred to another vacuum chamber for perovskite deposition. The latter is equipped with four evaporation sources (Vaksis) fitted with ceramic crucibles and independent temperature controllers and shutters (see Figure S6). A dedicated QCM sensor is installed above each source plus one close to the substrate for the overall deposition rate measurement (total of 5 QCM sensors). All the sources were individually calibrated for its respective material. During the perovskite deposition, the individual QCM reading for the 4 materials were kept stable to the following values: 0.26 Å/s for CsBr, 0.20 Å/s for MAI, 0.80 Å/s for FAI and 1.00 Å/s for PbI_2. More accurate rates can be estimated with the measurement of cross-contamination. To do so, the recording of every source was measured with its respective shutter closed, while all the rest were open. These corrections result in rates of 0.36 Å/s for CsBr, 0.40 Å/s for MAI, 1.00 Å/s for FAI, 1.00 Å/s for PbI_2.The chamber was evacuated to a pressure of 10^{-6} mbar, and the perovskite films were then obtained by simultaneous evaporation of the four precursors. The increase of temperature of the evaporation sources was started when the pressure reached $6 \cdot 10^{-6}$ mbar. During the deposition, the pressure of the chamber was kept at $3 - 5 \cdot 10^{-5}$ mbar. The optimum deposition temperatures were found to be ~ 425 ºC for the CsBr, ~ 100 ºC for the MAI, ~ 165 ºC for the FAI and ~ 295 ºC for the PbI_2. Substrates were kept at room temperature during perovskite formation. After deposition of the perovskite layer, samples were transferred to the other vacuum chamber for HTL and p-HTL deposition. The devices were completed depositing a 10 nm thick film of pure TaTm and one of 40 nm of the p-HTL (TaTm:F_6-TCNNQ, 11 wt%). Devices were finished with the deposition of the metal top contact (gold, 100 nm thick) was deposited.

Characterization. Grazing incident X-ray diffraction (GIXRD) pattern were collected at room temperature on an Empyrean PANanalytical powder diffractometer using the Cu Kα1 radiation. Typically, three consecutive measurements were collected and averaged into single spectra. Scanning Electron Microscopy (SEM) images were performed on a Hitachi S-4800 microscope operating at an accelerating voltage of 2 kV over Platinum - metallized samples. The perovskite composition was determined by Energy dispersive X-Ray analysis (EDX) for the Pb/I/Br content and the Cs/MA/FA content was determined from their respective evaporation rates used in the perovskite deposition. Absorption spectra were collected using a fiber optics based

Avantes Avaspec2048 Spectrometer. Characterization of the solar cells was performed as follows. The external quantum efficiency (EQE) was estimated using the cell response at different wavelength (measured with a white light halogen lamp in combination with band-pass filters), where the solar spectrum mismatch is corrected using a calibrated Silicon reference cell (MiniSun simulator by ECN, the Netherlands). The current density-voltage (J-V) characteristics were obtained using a Keithley 2612A source measure under white light illumination using a solar simulator by Abet Technologies (model 10500 with an AM1.5G xenon lamp as the light source). The scan rate was 0.1 V/s. Before each measurement, the exact light intensity was determined using a calibrated Si reference diode equipped with an infrared cut-off filter (KG-3, Schott). Light intensity dependence measurements were done by placing 0.1, 1, 10, 20, 50% neutral density filters (LOT-QuantumDesign GmbH) between the light source and the device. The maximum power point tracking (MPPT) was evaluated inside a nitrogen filled glovebox illuminated under 1 sun illumination at 40 ºC with a Peltier temperature-control unit.

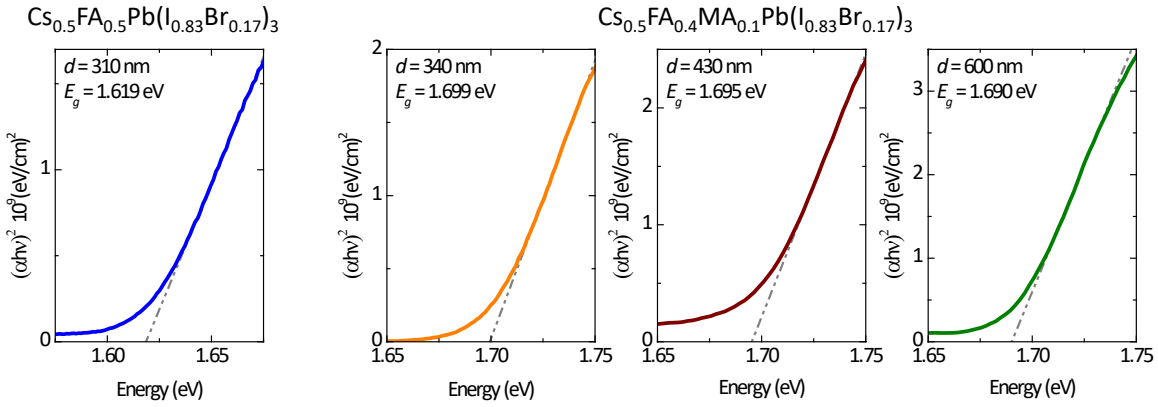

Figure S1. Bandgap estimation from fitting of the linear part of the Tauc plot for double- and triple-cation perovskites (the latter at different thicknesses).

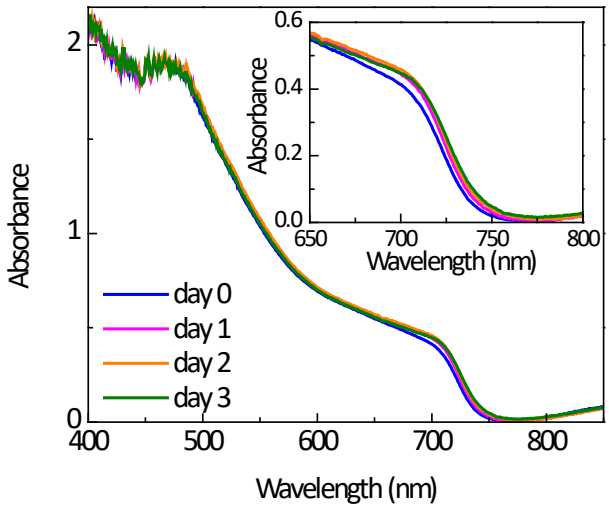

Figure S2. Evolution of the absorption spectrum at 25 ºC and 40% RH for the triple-cation perovskite $Cs_{0.5}FA_{0.4}MA_{0.1}Pb(I_{0.83}Br_{0.17})_3$.

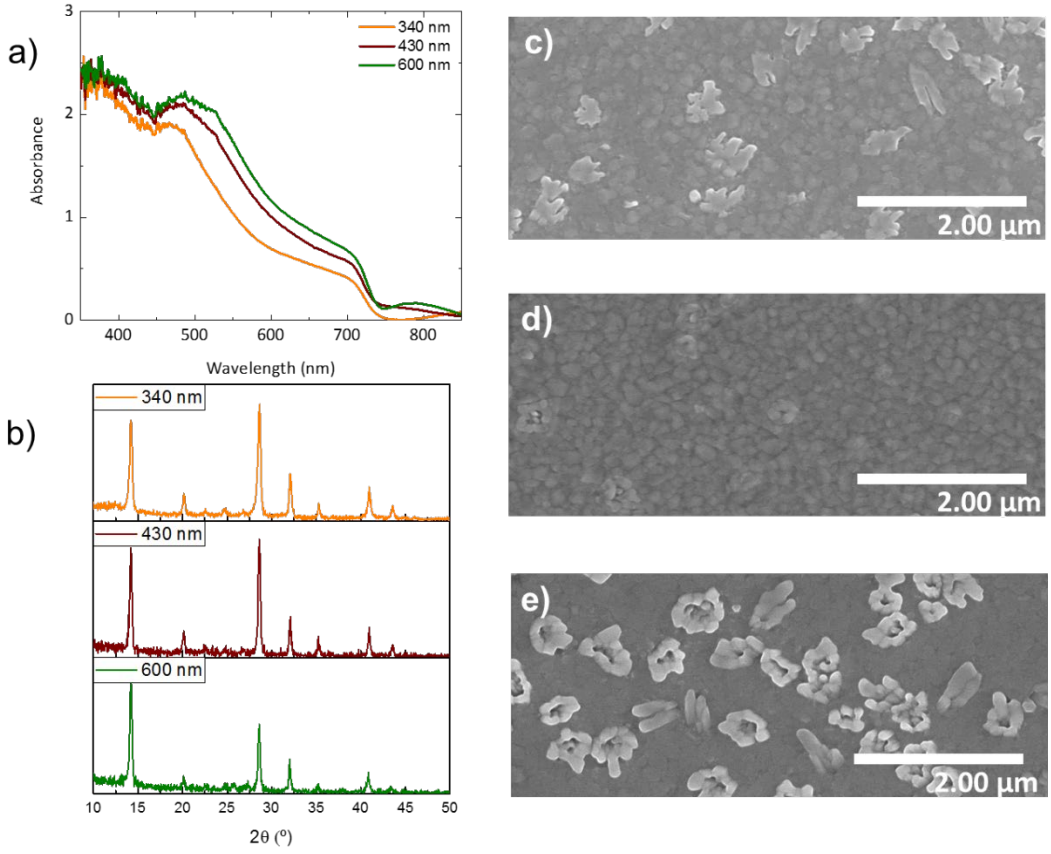

Figure S3. a) UV-Vis absorption spectra, b) XRD patterns and top view SEM images of $Cs_{0.5}FA_{0.4}MA_{0.1}Pb(I_{0.83}Br_{0.17})_3$ perovskite layers with increasing thickness: c) 340 nm, d) 430 nm and e) 600 nm.

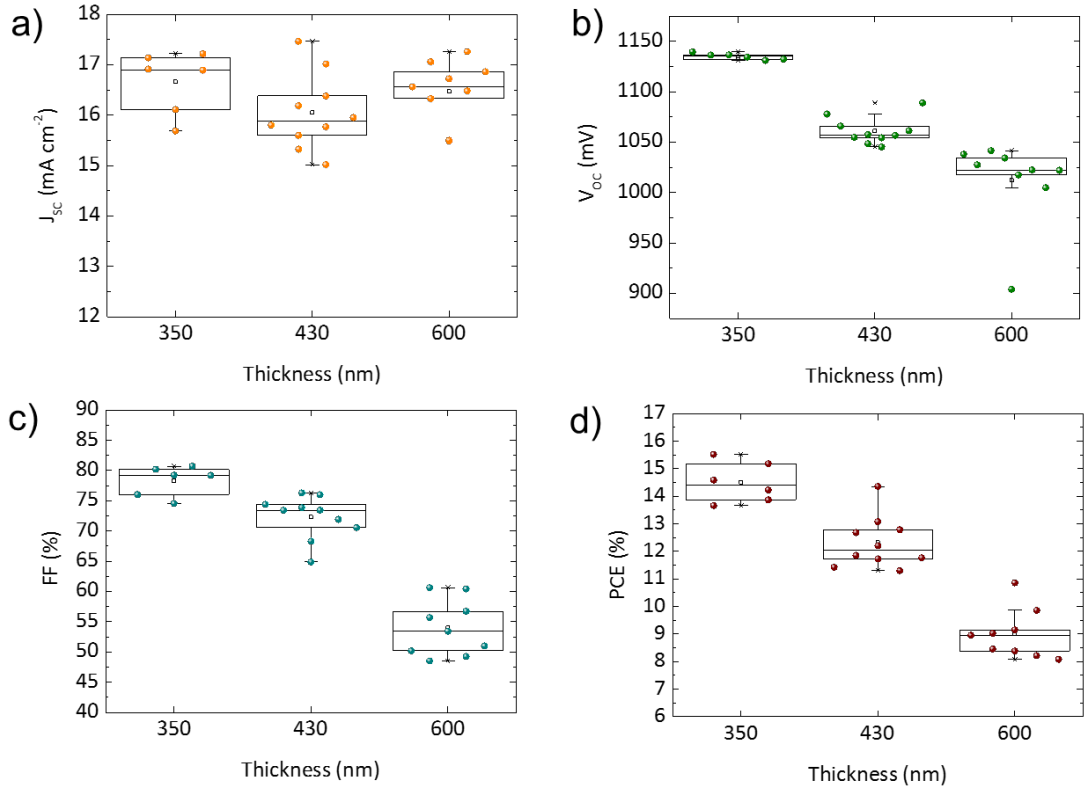

Figure S4. Statistics on the PV parameters for n-i-p devices with increasing thickness.

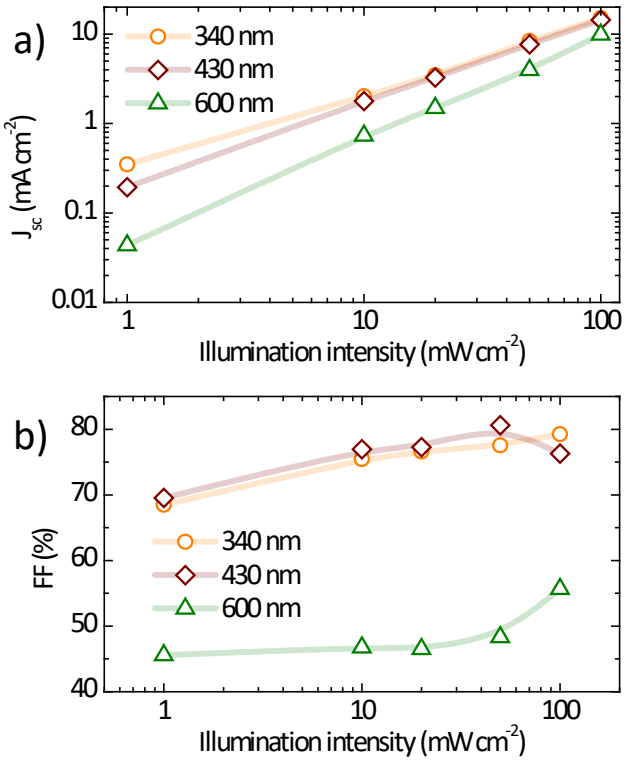

Figure S5. Plot of J_{sc} and FF vs light intensity for triple-cation perovskite solar cells at different absorber thickness.

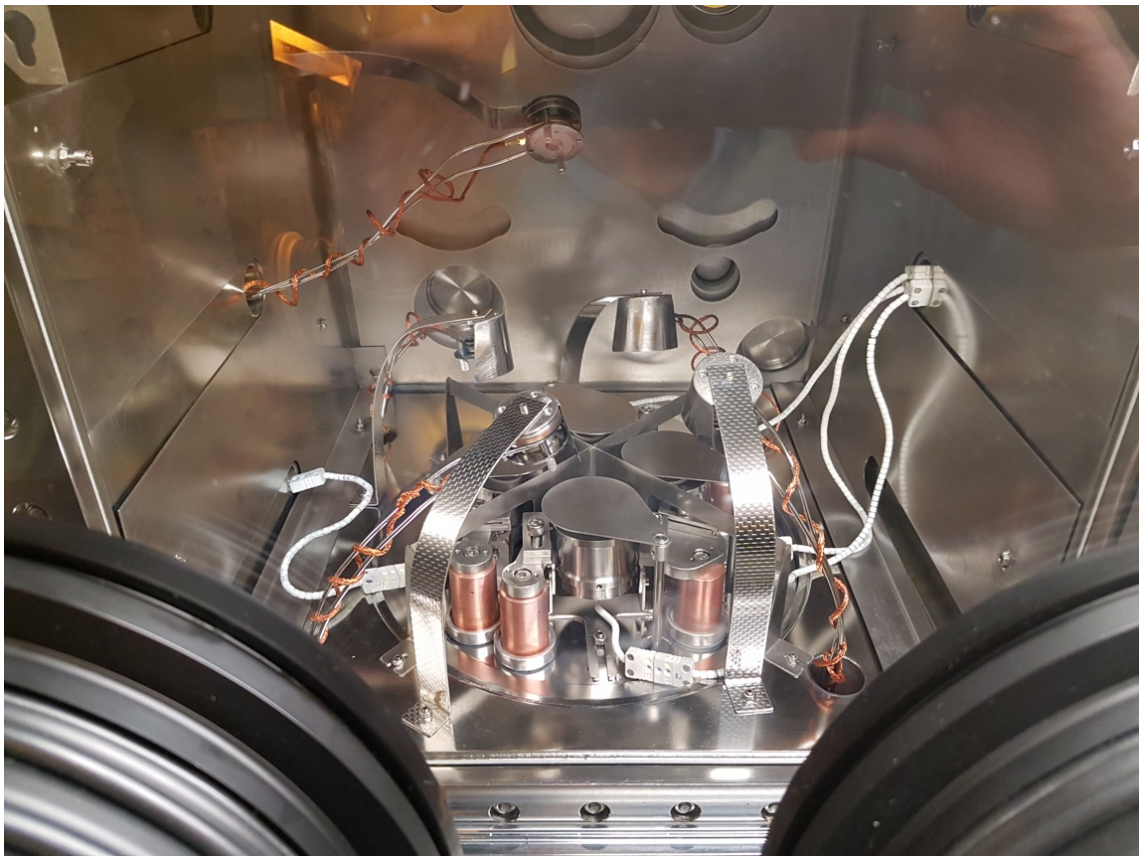

Figure S6. Photography of the evaporation chamber employed in this work.

ADVANCED ENERGY MATERIALS

Supporting Information

for *Adv. Energy Mater.,* DOI: 10.1002/aenm.201703506

Vacuum Deposited Triple-Cation Mixed-Halide Perovskite Solar Cells

*Lidón Gil-Escrig, Cristina Momblona, Maria-Grazia La-Placa, Pablo P. Boix, Michele Sessolo, and Henk J. Bolink**

Supporting Information

Vacuum deposited triple-cation mixed-halide perovskite solar cells

*Lidón Gil-Escrig,‡ Cristina Momblona,‡ Maria-Grazia La-Placa, Pablo P. Boix, Michele Sessolo and Henk J. Bolink**

Experimental section

Materials. Photolithographically patterned ITO coated glass substrates were purchased from Naranjo Substrates. Fullerene (C_{60}) was purchased from Sigma Aldrich. N1,N4-bis(tri-p-tolylphosphoranylidene)benzene-1,4-diamine (PhIm), N4,N4,N4",N4"-tetra([1,1'-biphenyl]-4-yl)-[1,1':4',1"-terphenyl]-4,4"-diamine (TaTm) and 2,2'-(Perfluoronaphthalene-2,6-diylidene) dimalononitrile (F_6-TCNNQ) were provided from Novaled GmbH. CH_3NH_3I (MAI) was purchased from Lumtec, $NH_2CH{=}NH_2I$ (FAI) from Dyesol, CsBr and PbI_2 from Tokyo Chemical Industry CO (TCI). All materials were used as received.

Device preparation. ITO-coated glass substrates were subsequently cleaned with soap, water and isopropanol in an ultrasonic bath, followed by UV-ozone treatment. They were transferred to a vacuum chamber integrated into a nitrogen-filled glovebox and evacuated to a pressure of 10^{-6} mbar for the charge extraction front contact layer deposition. The vacuum chamber for organic deposition is equipped with six temperature controlled evaporation sources (Creaphys) fitted with ceramic crucibles. The sources were directed upwards with an angle of approximately 90° with respect to the bottom of the evaporator. The substrate holder to evaporation sources distance is approximately 20 cm. Three quartz crystal microbalance (QCM) sensors are used, two monitoring the deposition rate of each evaporation source and a third one close to the substrate holder monitoring the total deposition rate. For thickness calibration, we first individually sublimed the charge transport materials and their dopants (TaTm and F_6-TCNNQ, C_{60} and PhIm). A calibration factor was obtained by comparing the thickness inferred from the QCM sensors with that measured with a mechanical profilometer (Ambios XP1). Hence these materials were co-sublimed at temperatures ranging from 135-160 ºC for the dopants to 250 ºC for the pure charge transport molecules, and the evaporation rate was controlled by separate QCM sensors

and adjusted to obtain the desired doping concentration. In general, the deposition rate for TaTm and C_{60} was kept constant at 0.8 Å s^{-1} while varying the deposition rate of the dopants during co-deposition. Pure TaTm and C_{60} layers were deposited at a rate of 0.5 Å s^{-1}. 40 nm thick films of the n-doped electron-transport layer (n-ETL, C_{60}:PhIm, 60 wt%) capped with 10 nm of the pure C_{60} were deposited. After completion of the front contact, the chamber was vented with dry N_2 and the samples were transferred to another vacuum chamber for perovskite deposition. The latter is equipped with four evaporation sources (Vaksis) fitted with ceramic crucibles and independent temperature controllers and shutters (see Figure S6). A dedicated QCM sensor is installed above each source plus one close to the substrate for the overall deposition rate measurement (total of 5 QCM sensors). All the sources were individually calibrated for its respective material. During the perovskite deposition, the individual QCM reading for the 4 materials were kept stable to the following values: 0.26 Å/s for CsBr, 0.20 Å/s for MAI, 0.80 Å/s for FAI and 1.00 Å/s for PbI_2. More accurate rates can be estimated with the measurement of cross-contamination. To do so, the recording of every source was measured with its respective shutter closed, while all the rest were open. These corrections result in rates of 0.36 Å/s for CsBr, 0.40 Å/s for MAI, 1.00 Å/s for FAI, 1.00 Å/s for PbI_2.The chamber was evacuated to a pressure of 10^{-6} mbar, and the perovskite films were then obtained by simultaneous evaporation of the four precursors. The increase of temperature of the evaporation sources was started when the pressure reached $6 \cdot 10^{-6}$ mbar. During the deposition, the pressure of the chamber was kept at $3 - 5 \cdot 10^{-5}$ mbar. The optimum deposition temperatures were found to be ~ 425 ºC for the CsBr, ~ 100 ºC for the MAI, ~ 165 ºC for the FAI and ~ 295 ºC for the PbI_2. Substrates were kept at room temperature during perovskite formation. After deposition of the perovskite layer, samples were transferred to the other vacuum chamber for HTL and p-HTL deposition. The devices were completed depositing a 10 nm thick film of pure TaTm and one of 40 nm of the p-HTL (TaTm:F_6-TCNNQ, 11 wt%). Devices were finished with the deposition of the metal top contact (gold, 100 nm thick) was deposited.

Characterization. Grazing incident X-ray diffraction (GIXRD) pattern were collected at room temperature on an Empyrean PANanalytical powder diffractometer using the Cu Kα1 radiation. Typically, three consecutive measurements were collected and averaged into single spectra. Scanning Electron Microscopy (SEM) images were performed on a Hitachi S-4800 microscope operating at an accelerating voltage of 2 kV over Platinum - metallized samples. The perovskite

composition was determined by Energy dispersive X-Ray analysis (EDX) for the Pb/I/Br content and the Cs/MA/FA content was determined from their respective evaporation rates used in the perovskite deposition. Absorption spectra were collected using a fiber optics based Avantes Avaspec2048 Spectrometer. Characterization of the solar cells was performed as follows. The external quantum efficiency (EQE) was estimated using the cell response at different wavelength (measured with a white light halogen lamp in combination with band-pass filters), where the solar spectrum mismatch is corrected using a calibrated Silicon reference cell (MiniSun simulator by ECN, the Netherlands). The current density-voltage (J-V) characteristics were obtained using a Keithley 2612A source measure under white light illumination using a solar simulator by Abet Technologies (model 10500 with an AM1.5G xenon lamp as the light source). The scan rate was 0.1 V/s. Before each measurement, the exact light intensity was determined using a calibrated Si reference diode equipped with an infrared cut-off filter (KG-3, Schott). Light intensity dependence measurements were done by placing 0.1, 1, 10, 20, 50% neutral density filters (LOT-QuantumDesign GmbH) between the light source and the device. The maximum power point tracking (MPPT) was evaluated inside a nitrogen filled glovebox illuminated under 1 sun illumination at 40 ºC with a Peltier temperature-control unit.

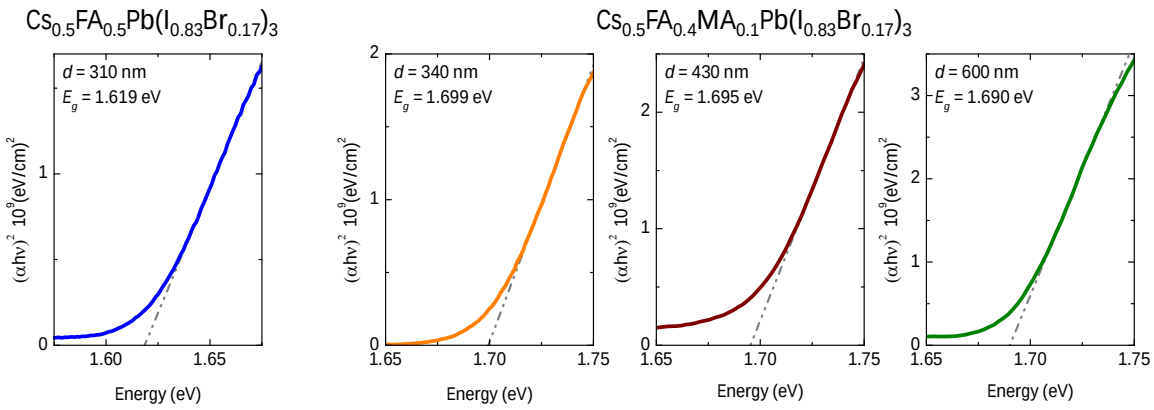

Figure S1. Bandgap estimation from fitting of the linear part of the Tauc plot for double- and triple-cation perovskites (the latter at different thicknesses).

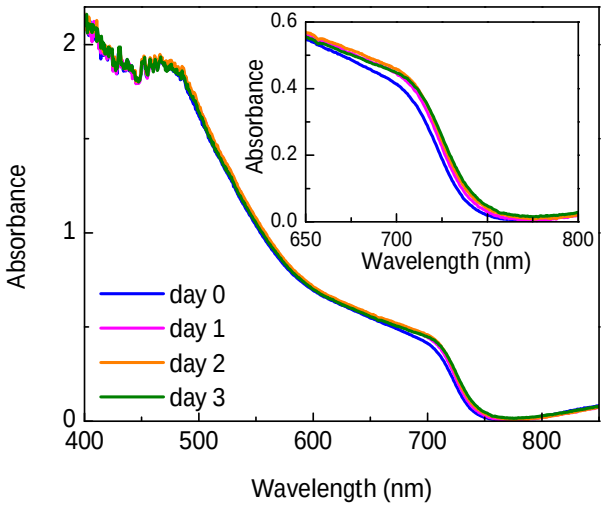

Figure S2. Evolution of the absorption spectrum at 25 ºC and 40% RH for the triple-cation perovskite $Cs_{0.5}FA_{0.4}MA_{0.1}Pb(I_{0.83}Br_{0.17})_3$.

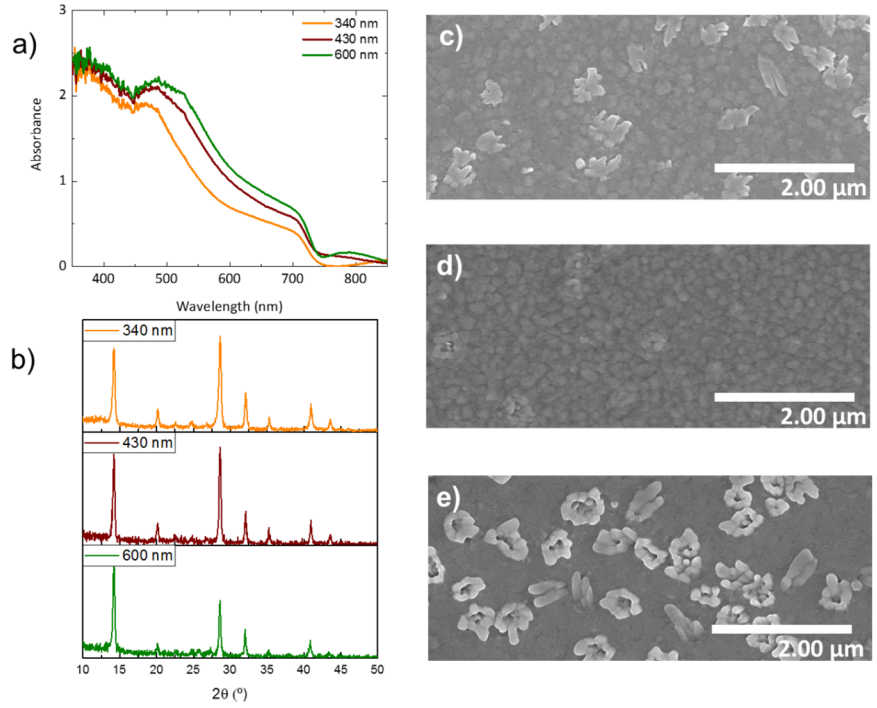

Figure S3. a) UV-Vis absorption spectra, b) XRD patterns and top view SEM images of $Cs_{0.5}FA_{0.4}MA_{0.1}Pb(I_{0.83}Br_{0.17})_3$ perovskite layers with increasing thickness: c) 340 nm, d) 430 nm and e) 600 nm.

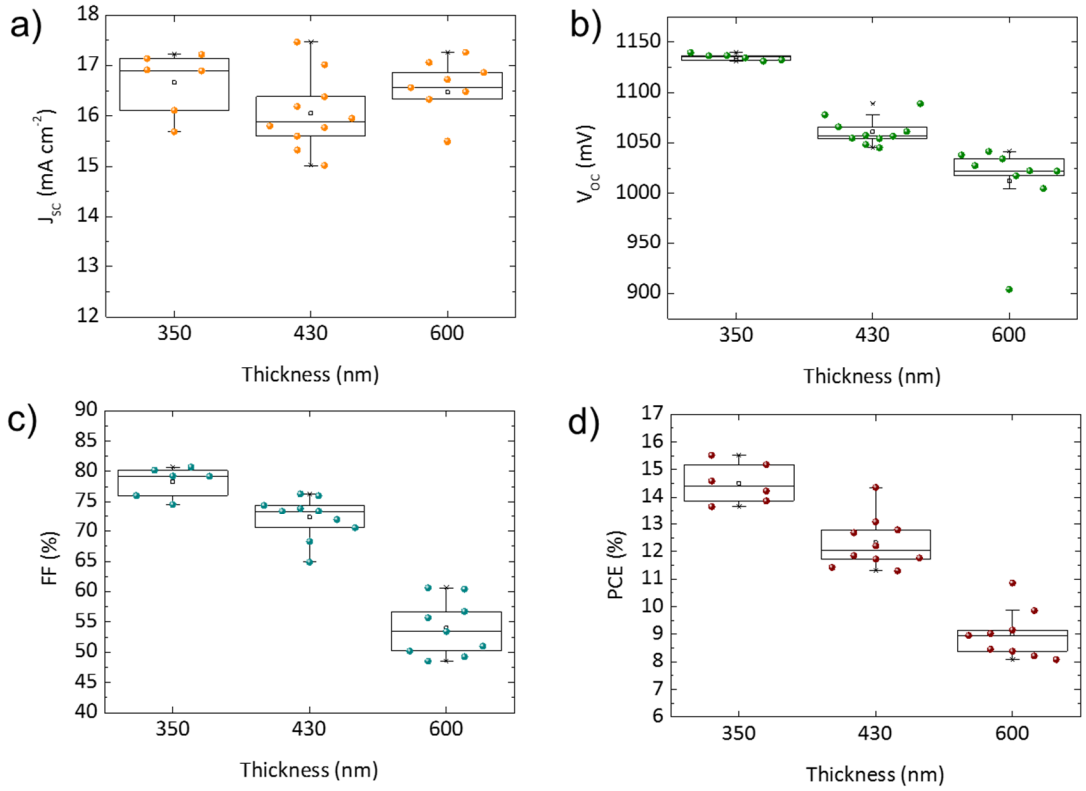

Figure S4. Statistics on the PV parameters for n-i-p devices with increasing thickness.

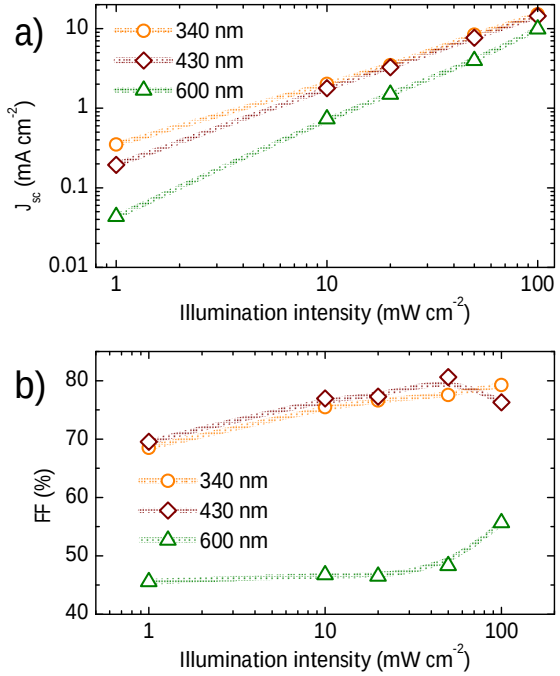

Figure S5. Plot of J_{sc} and FF vs light intensity for triple-cation perovskite solar cells at different absorber thickness.

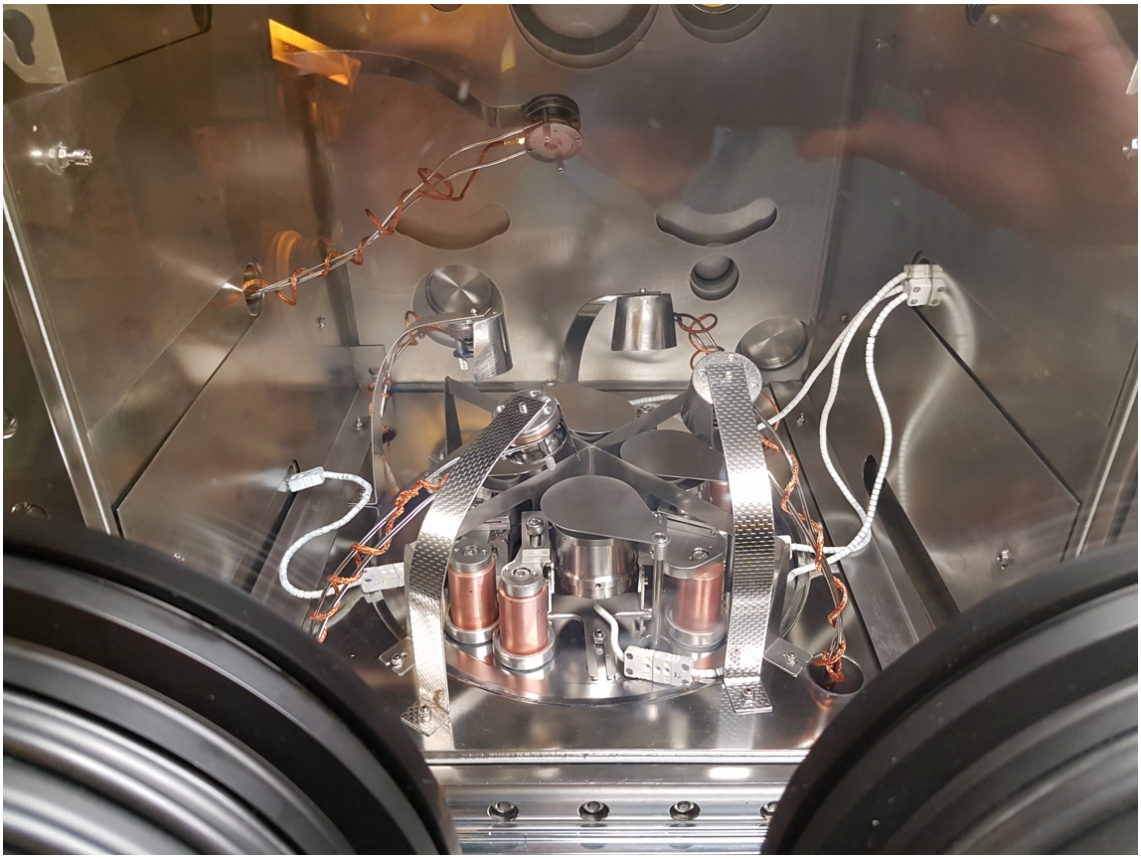

Figure S6. Photography of the evaporation chamber employed in this work.